European Radiology (2020) 30:1770–1779
https://doi.org/10.1007/s00330-019-06514-z

NUCLEAR MEDICINE

ZTE MR-based attenuation correction in brain FDG-PET/MR: performance in patients with cognitive impairment

Brian Sgard[1,2] · Maya Khalifé[3] · Arthur Bouchut[3] · Brice Fernandez[4] · Marine Soret[1,2] · Alain Giron[2] · Clara Zaslavsky[5] · Gaspar Delso[6] · Marie-Odile Habert[1,2] · Aurélie Kas[1,2]

Received: 22 May 2019 / Revised: 28 August 2019 / Accepted: 15 October 2019 / Published online: 20 November 2019

Abstract

Objective One of the main challenges of integrated PET/MR is to achieve an accurate PET attenuation correction (AC), especially in brain acquisition. Here, we evaluated an AC method based on zero echo time (ZTE) MRI, comparing it with the single-atlas AC method and CT-based AC, set as reference.

Methods Fifty patients (70 ± 11 years old, 28 men) underwent FDG-PET/MR examination (SIGNA PET/MR 3.0 T, GE Healthcare) as part of the investigation of suspected dementia. They all had brain computed tomography (CT), 2-point LAVA-flex MRI (for atlas-based AC), and ZTE-MRI. Two AC methods were compared with CT-based AC (CTAC): one based on a single atlas, one based on ZTE segmentation. Impact on brain metabolism was evaluated using voxel and volumes of interest–based analyses. The impact of AC was also evaluated through comparisons between two subgroups of patients extracted from the whole population: 15 patients with mild cognitive impairment and normal metabolic pattern, and 22 others with metabolic pattern suggestive of Alzheimer disease, using SPM12 software.

Results ZTE-AC yielded a lower bias (3.6 ± 3.2%) than the atlas method (4.5 ± 6.1%) and lowest interindividual (4.6% versus 6.8%) and inter-regional (1.4% versus 2.6%) variabilities. Atlas-AC resulted in metabolism overestimation in cortical regions near the vertex and cerebellum underestimation. ZTE-AC yielded a moderate metabolic underestimation mainly in the occipital cortex and cerebellum. Voxel-wise comparison between the two subgroups of patients showed that significant difference clusters had a slightly smaller size but similar locations with PET images corrected with ZTE-AC compared with those corrected with CT, whereas atlas-AC images showed a notable reduction of significant voxels.

Conclusion ZTE-AC performed better than atlas-AC in detecting pathologic areas in suspected neurodegenerative dementia.

Key Points

- *The ZTE-based AC improved the accuracy of the metabolism quantification in PET compared with the atlas-AC method.*
- *The overall uptake bias was 21% lower when using ZTE-based AC compared with the atlas-AC method.*
- *ZTE-AC performed better than atlas-AC in detecting pathologic areas in suspected neurodegenerative dementia.*

Keywords PET/MR · ZTE MRI · Attenuation correction · Fluoro-2-deoxy-D-glucose (FDG) · Neurodegenerative dementia

Brian Sgard and Maya Khalifé contributed equally to this work.

Electronic supplementary material The online version of this article (https://doi.org/10.1007/s00330-019-06514-z) contains supplementary material, which is available to authorized users.

✉ Brian Sgard
sgardbrian@gmail.com

[1] Department of Nuclear Medicine, Groupe Hospitalier Pitié-Salpêtrière Charles Foix, 75013, APHP, Paris, France

[2] Laboratoire d'Imagerie Biomédicale (LIB), Sorbonne Université, CNRS, INSERM, 75006 Paris, France

[3] Centre de NeuroImagerie de Recherche (CENIR), Institut du Cerveau et de la Moelle épinière (ICM), Paris, France

[4] Applications and Workflow, GE Healthcare, Orsay, France

[5] Department of Biophysics, Sorbonne Université, 75013 Paris, France

[6] Applications and Workflow, GE Healthcare, Cambridge, UK

Abbreviations

AAL	Automated anatomical labeling
AC	Attenuation correction
AC-PC line	Anterior commissure–posterior commissure line
AD	Alzheimer disease
CNN	Convolutional neural networks
DL	Deep learning
FDG	2-Fluoro-2-deoxy-D-glucose
FWE	Family-wise error
HU	Hounsfield unit
MNI	Montreal Neurological Institute
MR	Magnetic resonance
MRAC	Magnetic resonance–based attenuation correction
MRI	Magnetic resonance imaging
PET	Positron emission tomography
PSF	Point spread function
SPM	Statistical parametric mapping
SUV	Standard uptake value
TOF	Time of flight
UTE	Ultrashort time
ZTE	Zero time echo

Introduction

An important technical challenge of integrated brain PET/MR is achieving an accurate PET attenuation correction (AC) comparable with transmission-based computed tomography (CT) [1]. It is a major prerequisite for fluoro-2-deoxy-D-glucose (FDG) PET to be quantitative, especially in the context of early diagnosis of Alzheimer disease (AD). In current PET/MR scanners, AC is accomplished by generating an MRI-based surrogate CT from which AC-maps are derived [2]. MR-based AC methods (MRAC) implemented on clinical PET/MR scanners, use a 2-point Dixon MR which is segmented into four tissues classes (i.e., lung, air, fat, and soft tissue) with predefined attenuation coefficients. In brain studies, it is supplemented by the use of a single average CT template image generated from the average of normal head CT scans (atlas-based AC) or substituted by an ultrashort or zero echo time (UTE/ZTE) MRI to capture bone information. Atlas-based AC method relies on registering the single CT template to patient MR to correct brain metabolism from bone attenuation due to the skull. However, this approach has shown some limitations when applied to unusual head anatomies [3–6], and is highly dependent on image registration quality of the CT template to individual MR image. ZTE-based AC methods have been suggested as good candidates for accurate and subject-specific AC as ZTE MRI provides signal in tissue with short T2*, enabling the capture of air and bone information [6]. They demonstrated promising performances compared with the atlas-AC in a small number of subjects [5–8]. However, their performance on brain metabolism measurements in patients with neurodegenerative diseases has not been evaluated so far. Additionally, although ZTE-AC globally improved AC compared with the atlas-AC, a remaining bias was reported in the nasal sinus cavity and temporal bones as these structures, containing bone-air-soft tissue interfaces, were not correctly segmented due to partial volume effect [9].

In this work, we aim to evaluate ZTE-AC in 50 patients referred for cognitive impairment, by comparing it with the atlas-AC method implemented in a clinical setting and to CT-AC method set as reference. The ZTE-AC generation algorithm used here was modified to improve the segmentation in the sinus and temporal bones and detailed in the "Materials and methods" section.

Materials and methods

Population

Fifty consecutive patients (70 ± 11 years old, 28 men) examined at our institution between 2016 and 2017, and fulfilling the following criteria, were included: (1) brain FDG-PET/MR scan (SIGNA 3T PET/MR, GE Healthcare) performed in the context of neurocognitive disorders investigation; (2) available brain CT scan without iodinated contrast agent injection; (3) no skull, face, or neck surgery or injury between CT and PET/MR examinations. All data were extracted from the database of the Pitié-Salpêtrière Hospital, Paris, France, and data use was approved by the French authority for the protection of privacy and personal data in clinical research (CNIL, approval no. 2111722). This study was performed according to the principles of the Declaration of Helsinki.

PET/MR acquisition

Brain PET/MR was acquired 30 min after the injection of 2 MBq/kg FDG. MR imaging included 3D T1-weighted inversion-recovery fast spoiled gradient echo acquisition, 3D FLAIR; 3D susceptibility-weighted MRI and axial diffusion-weighted imaging. Scanning time also included a 20-min single-bed position PET emission scan.

To correct for photon attenuation, a 2-point Dixon (LAVA-Flex) T1-weighted MRI (axial acquisition TR = 4 ms; TE = 1.12 and 2.23 ms; flip angle 5°; slice thickness 5.2 mm, with a 2.6-mm overlap; 120 slices; pixel size of 1.95 × 1.95 mm^2, acquisition time 15 s) was acquired yielding water, fat, and in-phase and out-phase contrasts. A ZTE MRI was acquired with the following parameters: 3D center-out radial acquisition; TR = 390 ms; TE = 0 ms; flip angle 0.8°; slice thickness 2.4 mm; voxel size 2.4 × 2.4 × 2.4 mm^3; field of view 26.4 × 26.4 m^2; bandwidth ± 62.5 kHz; acquisition time 40 s.

AC map processing

Three AC maps were created for each patient: one attenuation image derived from a CT scan (CT-AC map) set as reference, and two MR-based images (ZTE- and atlas-based AC maps) being evaluated.

First, an atlas-AC map was generated, as previously described [10], using a single atlas-based AC method corresponding to a non-rigid registration of an average CT template on the Dixon in-phase image using the implemented process on the PET/MR scanner.

A second AC map was generated from ZTE MRI segmentation (ZTE-AC). An offline post-processing pipeline provided by the manufacturer was used to generate bone tissue estimates from the acquired ZTE data based on the method proposed by Wiesinger et al [11], including sinus-edge correction described in Delso et al [12] and Yang et al [13]. First, bias correction was applied to homogenize ZTE signal intensity over the patient tissue, followed by an intensity normalization by the value of the soft tissue peak in the intensity histogram (intensity of air voxels centered at 0, intensity of soft tissue voxels centered at 1) [14]. Second, a three-class tissue segmentation (bone, air, and tissue) was performed using histogram-based thresholding as follows: air voxels have an intensity lower than 0.25, soft tissue voxels have an intensity higher than 0.85, and bone voxels are in between. Finally, an attenuation coefficient was assigned to each tissue class to generate a pseudo-CT. A value of − 1000 HU was used for air and 42 HU was used for soft tissue. The assumption that attenuation coefficients of soft tissue are uniform is acceptable even in the case of brain atrophy since attenuation coefficients of cerebral spinal fluid (15 HU), gray matter (37–45 HU), and white matter (20–30 HU) are not significantly different. Voxels classified as bone were assigned density values of 42 + 2400·(1 − I_{ZTE}) HU, where I_{ZTE} represents the normalized ZTE voxel intensity. This relationship linking ZTE intensity to CT HU values, although not determined on this population, was published in Wiesinger et al [15]. Additionally, a number of sensitive anatomical regions were selected to impose additional constraints on the segmentation, namely to prevent false-positive bone voxels in areas affected by partial volume effect as explained in Delso et al [12]. These regions were identified in previous studies [9, 13] and were known to pose difficulties to pure intensity-based bone segmentation. The paranasal sinuses are arguably the most relevant of these regions, due to their complex hollow structure. Another challenging region is the temporal bones, where the air of the ear canal and mastoid cells are in close proximity with some of the densest sections of bone in the body.

CT-based AC method was set as the gold standard as it is used to correct for the attenuation of PET 511-keV photons in PET/CT systems. A non-enhanced, low-dose head CT (120 kVp, 50 mAs) was collected for each patient from brain PET/CT examinations performed in our department with either a Gemini GXL 16, Philips PET/CT system (3 mm slice thickness, 6.8 mm in plane pixel size), or a Biograph mCT Flow, Siemens PET/CT system (2 mm slice thickness, 5.9 mm in plane pixel size). The quality control of CT component of the PET/CT systems (CT number, uniformity, image noise, and image artifacts) was carried out regularly (three times a year). The time interval between CT scan and PET/MR examination was 16 ± 25 months (range, 0–134 months). So, for each patient, CT and MR images were compared by a physician trained in brain imaging to ensure that no anatomical discrepancies were found between MR and CT scans (no skull deformation, post-operative sequelae, or brain lesion). CTAC maps were created after registering CT images to ZTE MR images using an affine registration based on mutual information maximization algorithm with the MIPAV software (CIT-NIH) and visually checked to detect any spatial mismatch [16]. In addition, as attenuation depends on both photon energy and density of absorbing material, we used the bilinear conversion method based on the attenuation of water and cortical bone to convert linear attenuation coefficients from CT energies (120 keV) to 511-keV PET photon energy [17, 18] to generate the CTAC map used as the gold standard [19].

All AC maps (Suppl. Fig. 1) were then processed as follows with MATLAB software (MathWorks Inc.). As described in Zhang et al [20] and Eldib et al [21], the attenuation maps of non-patient objects within the FOV (coils, bed, and all surrounding materials) were added to AC maps using the PET Recon toolbox provided by GE Healthcare. AC maps were smoothed with a Gaussian filter kernel of 10-mm full-width at half-maximum, which is the default smoothing applied on the atlas-AC map by the manufacturer. Then, PET images were reconstructed with each AC map generating three images per patient (PET_{ATLAS}, PET_{ZTE}, and PET_{CT} corrected with Atlas-AC, ZTE-AC, and CT-AC, respectively) using the following parameters: Ordered Subsets Expectation Maximization algorithm integrating TOF, PSF modeling, attenuation and scatter correction with 8 iterations and 28 subsets, a FOV of 300 × 300 mm^2, and a voxel size of 1.17 × 1.17 × 2.78 mm^3.

Quantitative analysis

PET images were spatially normalized in the Montreal Neurological Institute (MNI) space with SPM12 (http://www.fil.ion.ucl.ac.uk/spm/software/spm12) and processed to generate maps of mean relative difference and standard deviation for the 50 patients and each AC method as follows:

$$Diff_{MRAC}\,(\%) = \frac{(PET_{MRAC} - PET_{CT})}{PET_{CT}} \times 100$$

Additionally, MRAC methods were quantitatively assessed with volumes of interest (VOIs). PET images were normalized in intensity by dividing voxel activity by the mean pons uptake, yielding images of SUV ratios (SUVR). The pons was chosen as its metabolism is relatively preserved in cognitive disorders [22] and not significantly modified by MRAC in preliminary analyses. Ninety cortical and subcortical VOIs from the Automated Anatomical Labeling brain atlas (AAL, http://www.gin.cnrs.fr/fr/outils/aal-aal2/) [23] were applied on SUVR images to extract regional values from PET_{ATLAS} ($SUVR_{ATLAS}$), PET_{ZTE} ($SUVR_{ZTE}$), and PET_{CT} ($SUVR_{CT}$). The percentage of relative (ΔSUVR) and absolute (|ΔSUVR|) differences were computed with respect to PET_{CT}, as follows:

$$\Delta SUVR\ (\%) = 100 \times \frac{(SUVR_{MRAC} - SUVR_{CT})}{SUVR_{CT}}$$

PET_{ATLAS}, PET_{ZTE}, and PET_{CT} images—previously spatially normalized, normalized in intensity, and smoothed—were also compared on voxel basis with paired *t* tests, using the following contrasts: (i) $PET_{ATLAS/ZTE} > PET_{CT}$ to exhibit cortical regions whose metabolism is overestimated by MRAC in comparison with CTAC; (ii) $PET_{CT} > PET_{ATLAS/ZTE}$ to explore regions with statistically significant metabolism underestimation. The threshold was set to $p < 0.001$ corrected for multiple comparisons with the family-wise error (FWE) method at the voxel level. Only clusters bigger than 300 voxels were considered.

Finally, to test the impact of MRAC on between-groups analyses, two subgroups of patients were extracted from the whole population. Patient selection was established on the basis of suspected diagnosis and/or prominent symptoms at presentation, and metabolic profile on PET_{CT} images interpreted visually by a physician with 15 years' experience. Two groups were defined: (i) 22 patients with moderate to severe hypometabolism in associative posterior cortex compatible with Alzheimer's disease (73 ± 8.1 years old; 12 men); (ii) 15 patients with mild cognitive impairment whose cortical metabolism was considered normal at visual inspection (67 ± 16.1 years old; 9 men). Between-groups comparisons were conducted with two-sample *t* tests with PET_{ATLAS}, PET_{ZTE}, and PET_{CT} providing three SPM T maps that were subsequently compared, and the results obtained with CTAC being used as reference. Age and sex were set as covariates. Considering the small sample size, the threshold was lowered at $p < 0.001$ uncorrected, with a minimal cluster size of 300 voxels.

Results

VOI analysis results are detailed in Fig. 1, displaying the mean SUVR difference and standard deviation (SD). Over all VOIs, the ZTE-based AC yielded a lower bias (|ΔSUVR| = 3.6 ± 3.2%) than the atlas method (|ΔSUVR| = 4.5 ± 6.1%). The atlas-AC also yielded higher interindividual (6.8% versus 4.6% for ZTE-AC) and inter-regional variability (2.6% versus 1.4% for ZTE-AC) in comparison with the ZTE method.

Maps of mean and SD relative difference between MRAC and CTAC are shown in Fig. 2. They show that atlas-based AC overestimates glucose metabolism in the bilateral frontoparietal cortex extending to the temporoparietal junction. The highest overestimation was found in regions close to the vertex, mainly the middle frontal gyrus (ΔSUVR = 4.3 ± 6.5%), supplementary motor area (ΔSUVR = 8.2 ± 7.3%), bilateral paracentral lobule (ΔSUVR = 7.9 ± 6.9%), and superior parietal cortex (ΔSUVR = 7.4 ± 13.0%) as shown in Fig. 2. These results were confirmed by the SPM approach ($p < 0.001$ FWE corrected; Fig.3 and Supp. table 2). Conversely, the atlas-AC underestimates the regional metabolism below the anterior commissure–posterior commissure (AC-PC) line, in the inferior temporal, occipital, orbitofrontal cortices, the temporal pole, and the cerebellum (Fig. 2). The underestimation reached statistical significance in the cerebellum only ($p < 0.001$ FWE corrected; Fig. 3 and Supp. table 2). SD maps revealed high interindividual variability in parietotemporal cortex especially in the superior parietal cortex (12.2%) and the right angular gyrus (11.4%) (Figs. 1, 2).

Regarding the ZTE-based AC, the metabolism was moderately underestimated through the whole cortex (Fig. 2). Voxel-wise statistical significance was observed in the cerebellum, and the fusiform gyrus extending through the parietooccipital cortex, as well as in a very small cluster in the prefrontal dorsolateral cortex ($p < 0.001$ FWE corrected; Fig. 3, Supp. table 2). ΔSUVR was − 4.2 ± 4.6% in the cuneus, − 4.9 ± 7.4% in the superior parietal cortex, and − 1.3 ± 2.6% in the cerebellum. No regional metabolism overestimation was found with ZTE-AC. Interindividual variability was lower than that of atlas-based AC (Figs. 1 and 2).

SPM comparisons between patients with normal vs. abnormal PET are shown in Fig. 4 and Supp. table 3. When performed with PET_{CT}, SPM analysis revealed a large hypometabolism of the bilateral posterior associative cortex: the posterior cingulate in the patients with metabolic pattern suggestive of AD ($p < 0.001$). The same comparison performed with PET_{ZTE} provided significant clusters of slightly smaller size and lower *t* scores but similar topographies, whereas only scattered clusters were found in the left posterior junction and the cuneus when using atlas-based AC.

Discussion

We evaluated the impact of AC algorithms based on CT-atlas and ZTE-MRI on brain metabolism in 50 patients explored for cognitive impairment with PET/MRI. VOIs and voxel-based

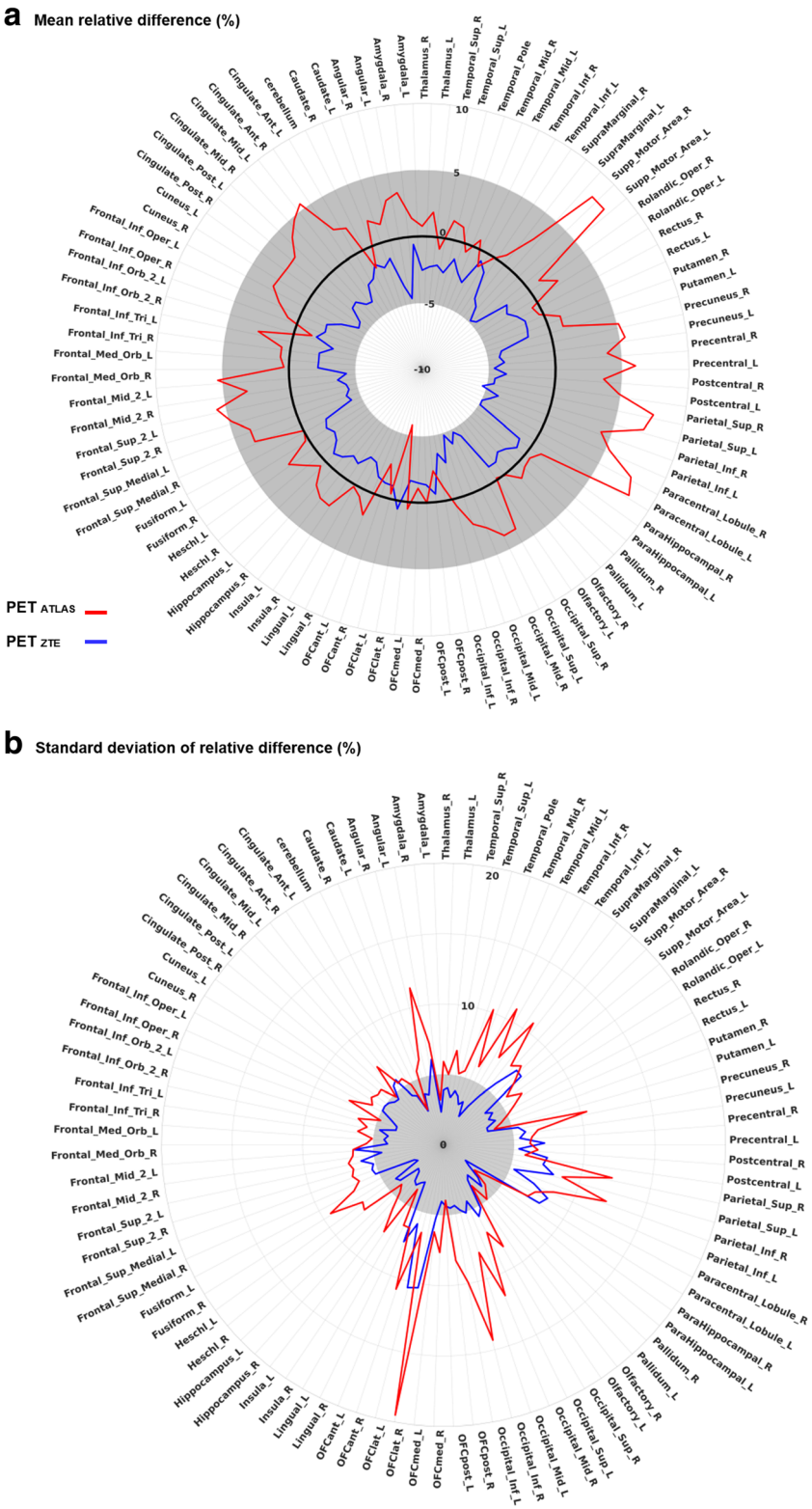

Fig. 1 Mean SUVR relative difference (**a**) and standard deviation (**b**) in PET_{ATLAS} (in red) and PET_{ZTE} (in blue) in comparison with PET_{CT}. Differences were calculated in 90 VOIs using the AAL toolbox [23] and averaged over the 50 patients. In each VOI, the relative difference is normalized by SUVR in PET_{CT}. In (**a**), the full black line depicts the zero line and the gray ring indicates the [− 5, + 5] % interval. In (**b**), the gray disk indicates the [0, + 5] % interval. VOIs are listed in Suppl. table 1

analyses showed that ZTE-AC method performed better than the atlas-AC, yielding a moderate bias on metabolism measurements with low interindividual and inter-regional variabilities.

PET_{ATLAS} showed a significant positive bias in the regions located above the AC-PC line especially those close to the vertex, and a negative bias in the lower regions, especially the cerebellum. Such variability across regions might result

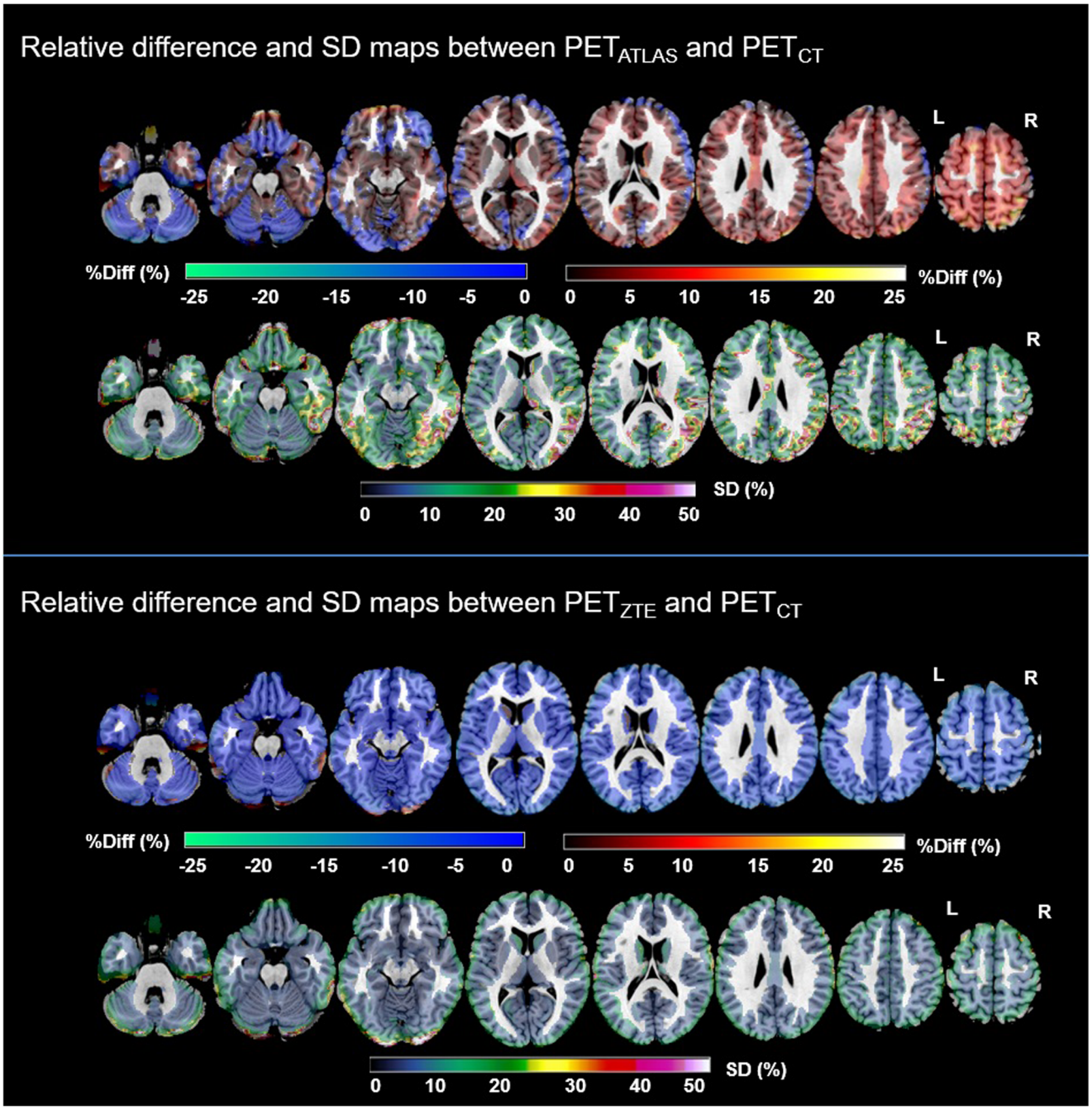

Fig. 2 Maps of SUV relative difference and standard deviation of relative difference. Map of SUV mean relative difference (%Diff, upper) and standard deviation (SD, lower) between $PET_{ATLAS/ZTE}$ and PET_{CT} overlaid on T1-weighted MRI template in the MNI space

in a difficult interpretation of FDG-PET data especially when the cerebellum is used as reference for the activity normalization of the whole brain. Similarly, the interindividual variability was significantly higher with PET_{ATLAS} than the one measured with PET_{ZTE}, mainly in the parietotemporal junction that is one of the earliest regions involved in Alzheimer's disease. The limits of the atlas-AC method may be explained by the use of average healthy subjects' CT scans to generate AC maps, which cannot take into account the specificity of head anatomies. For example, the cranial vault thickness is often overestimated on AC maps, especially in the upper part of the frontal and parietal bones, which could cause metabolism overestimation of the adjacent cortex; on the contrary, the rostral portion of the frontal bone, the mastoid part of the temporal bone, and the skull base may be underestimated or missing, possibly leading to metabolism underestimation observed in the orbitofrontal, inferior temporal cortices, and cerebellum.

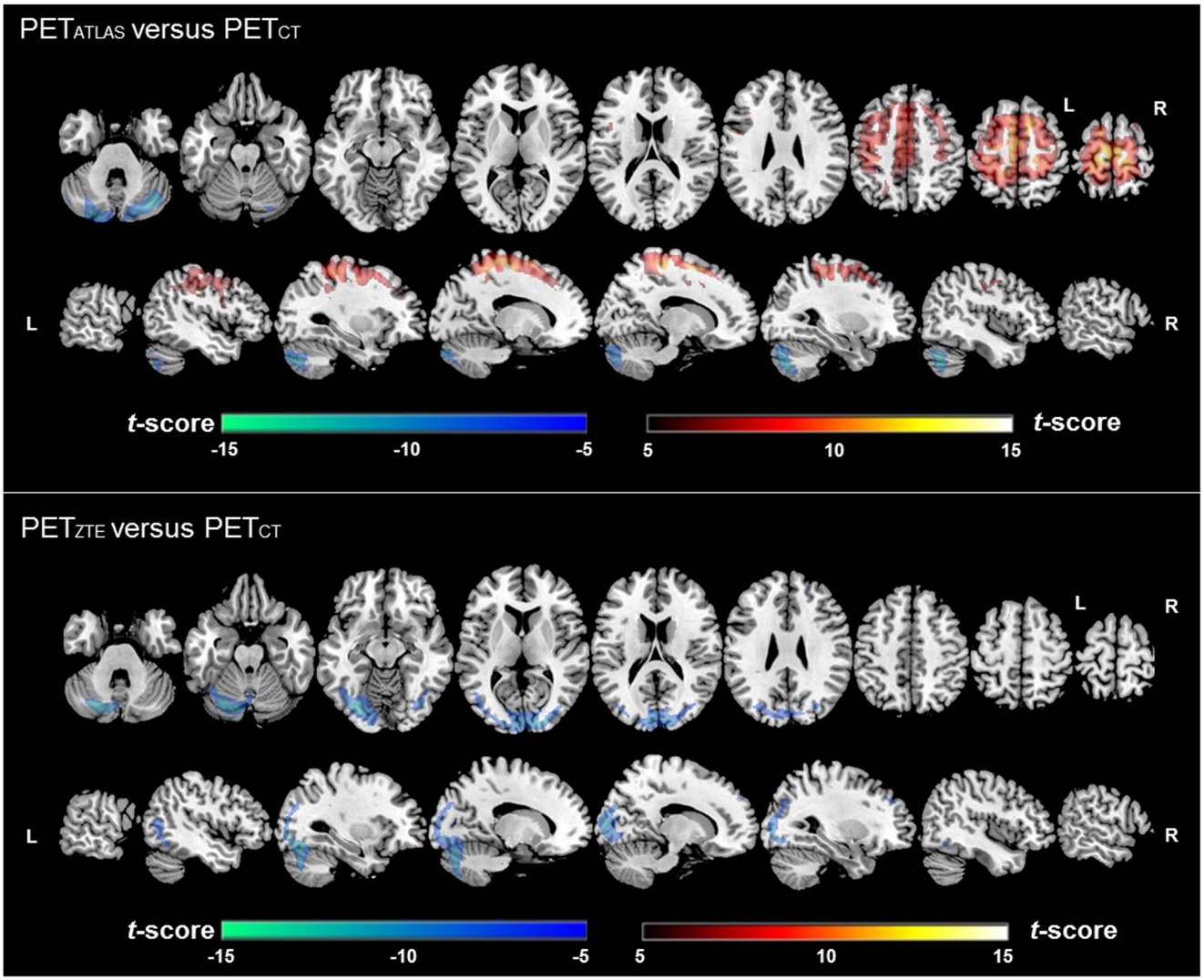

Fig. 3 SUV comparison between PET_{ZTE} and PET_{ATLAS} compared with PET_{CT}: SPM results. Paired *t* test comparisons between PET_{ATLAS} and PET_{CT} (upper) and between PET_{ZTE} and PET_{CT} (lower) in MNI space. Statistical maps were thresholded for significance at $p < 0.001$ FWE-corrected at the voxel level. $PET_{ATLAS/ZTE} > PET_{CT}$ are shown in hot colors with positive values to highlight the brain regions with significant metabolism overestimation and $PET_{ATLAS/ZTE} < PET_{CT}$ are shown in cold colors with negative values to highlight the brain regions with significant metabolism underestimation. The metabolism overestimation/underestimation is in regard with the PET_{CT} gold standard

When using the ZTE-AC method, the bias decreases by 21% with respect to atlas-AC. ZTE-AC yielded a lower bias (3.6 ± 3.2%) and a reduced interindividual (4.6% versus 6.8%) and inter-regional (1.4% versus 2.6%) variabilities. ZTE-AC yielded a moderate metabolic underestimation mainly in the occipital cortex and cerebellum. On ZTE-AC maps, the skull, mastoid, and the skull base were correctly depicted. Furthermore, the improved ZTE segmentation algorithm showed good performance in the regions reported as troublesome: air cavities in the frontal sinus, maxillary sinus, and nasal fossa were correctly segmented in ZTE-AC maps as well as the mastoid cells. Nonetheless, air cells and segments of the ethmoid bone were sometimes replaced by soft tissues. The occipital bone was sometimes thinner than that observed in CT scan, which may cause metabolism underestimation in the cerebellum.

In the multicenter evaluation of Ladefoged et al [2], the three major types of clinical feasibility MR-AC methods were selected for evaluation: template/atlas-based, maximum-likelihood reconstruction-based and segmentation-based AC (including a MR-AC method using an ultrashort time echo sequence (UTE)). All of the proposed methods had an average global performance within likely acceptable limits (± 5% of CT-based reference). However, the accuracy of ZTE-based AC was not evaluated in this panel. Our results are consistent with those of previous studies [5, 9, 13, 24], which found advantages of ZTE-AC over atlas-AC method, although their results were overall less pronounced. In Sekine et al [9] and Rezaei et al [25], ZTE-AC showed a lower bias (1.77 ± 1.41% and 0.2% ± 0.8%, respectively) than in our study, whereas it was larger (5.6 ± 3.5%) in Yang et al [13]. Sousa et al showed also that ZTE-

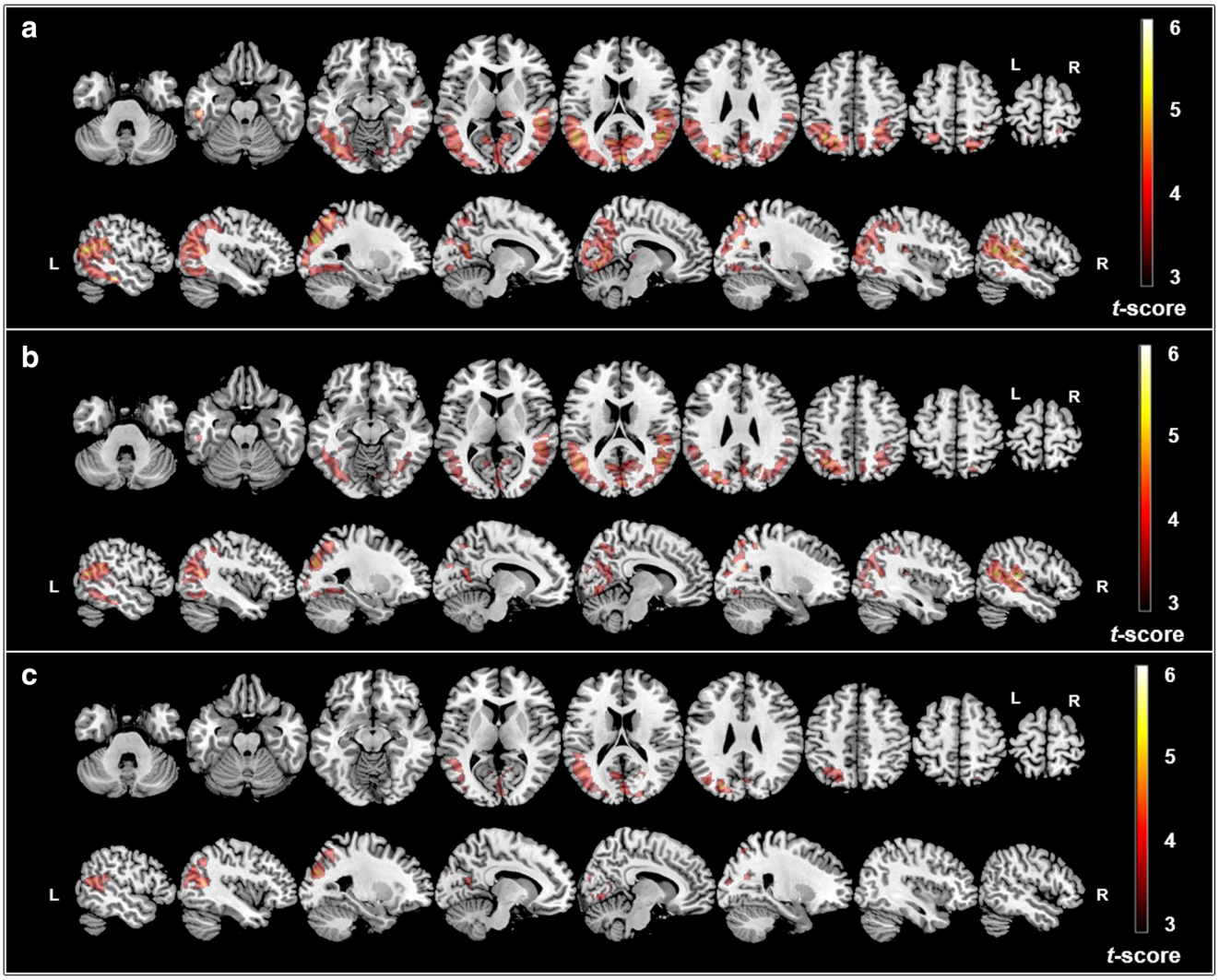

Fig. 4 Voxel-wise comparisons between normal and abnormal brain FDG-PET performed with PET_{CT} (**a**, reference), PET_{ZTE} (**b**), and PET_{ATLAS} (**c**). Two-sample *t* test between normal PET ($n = 15$) and abnormal PET suggestive of AD ($n = 22$) with (**a**) CT-AC (whose results are used as reference), (b) ZTE-AC, and (**c**) atlas-AC. Statistical maps were thresholded for significance at $p < 0.001$ uncorrected and cluster extent > 300. Results are displayed in neurological convention (left is left)

AC seems to be a more robust technique than atlas-AC for intra- and interpatient variabilities with 68-Ge transmission scan–based AC [24]. Furthermore, multi-atlas AC method was proven to be superior to the single-atlas method [4, 5], but has not yet been compared to ZTE-AC. The ZTE-AC algorithm used in this work was slightly different than the one used in previous studies. The segmentation algorithm had been improved to reduce segmentation errors in the sinus cavity and hollow temporal bones, which may explain differences in performance compared with previous reports. Also, the spatial resolution of ZTE images as well as the smoothing of PET images, which are different in the three studies, might be causing partial volume effect and thus tissue segmentation error in AC maps [8, 11].

Our aim was also to test the feasibility of ZTE-AC in clinical settings, with the shortest acquisition time and processing time possible. ZTE MR acquisition lasts 40 s and the time for PET reconstruction and attenuation correction is less than 5 min making it compatible with clinical constraints. ZTE-AC demonstrated better performances compared with the atlas-AC method in brain PET imaging. The large number of patients included allowed evaluating ZTE-AC in a heterogeneous sample of patients having mild to severe cognitive deficit and variable metabolic defects. In this context, the low interindividual variability of ZTE-AC denotes the ability of this method to successfully deal with subject specificity.

Additionally, voxel-based comparisons between patient subgroups suggested that SPM(t) maps generated with ZTE-AC were close to those obtained with CT-AC, whereas some clusters were missing in some key regions when using PET_{ATLAS} images, suggesting that ZTE-AC was more sensitive to detect pathological areas in suspected neurodegenerative dementia than atlas-AC, in our sample of patients.

This study has several advantages and limitations. Compared with previously published studies, this work included a large number of subjects and was the first one to specifically include patients with neurodegenerative disorders. The main limits of this work are its retrospective nature and the use of brain CT scans acquired on different CT systems. This limitation is common for retrospective PET/MRI studies where it is difficult to have both PET/MRI and PET/CT acquisition for the same patient in the same day. However, because spatial mismatch between the CT and MR images can occur leading to quantitative bias, a quality control was systematically performed in each patient for every coregistration process (between CT and MR images, and during spatial normalization). In addition, AC maps were smoothed with a Gaussian filter with full-width at half-maximum of 10 mm (which is the default blurring applied on the AC map by the vendor) to reduce this variability. Another limitation was the delay between PET/MRI and CT scans. For this, every CT and MR image was visually interpreted by a physician trained in brain imaging, to ensure that no morphological discrepancy was found between them. Only patients without skull abnormality or brain lesion appearing during the interval between CT and PET/MR examinations were included in this work.

Despite some limits of this study, the ZTE-AC method seemed to improve accuracy of the FDG metabolism quantification in this population referred for neurocognitive disorder investigation. It could be valuable to support and generalize interpretation of brain PET images with the lowest variability. This new AC method is readily applicable on SIGNA PET/MR and is now implemented on PET/MR software. Additionally, the use of ZTE-AC could be extended to other brain applications such as oncology.

Further improvement of ZTE-AC is expected from deep learning (DL) approaches with convolutional neural networks (CNN). DL has recently been applied to medical imaging with successful implementations showing promising results in segmenting brain structures, bone, and cartilage, and generating discrete-valued pseudo-CT scans from MR images. First results suggest it performs better than current clinical approaches (Dixon-based soft-tissue and air segmentation and atlas-based template registration) [26–28]. Recently, Ladefoged et al found that their UTE-based CNN improved quantification accuracy compared with UTE in pediatric brain tumors [29]. Large studies using prospective ZTE MR acquisition for deep learning MRAC are warranted.

Conclusion

The ZTE-based AC improved the accuracy of the metabolism quantification in PET—mainly in the regions close to the vertex—compared with the atlas-AC method. Our results suggest that the ZTE-AC method performed better than the atlas-AC method in patients with suspected cognitive dementia. Although ZTE-AC slightly decreased brain metabolism, it demonstrated a reduced inter-regional and interindividual variabilities. It seemed to improve the identification of regional hypometabolism in the context of cognitive impairment, and hence might be promising in other pathologies involving brain lesions.

Acknowledgements The authors would like to thank GE Healthcare for providing access to research tools and prototype pulse sequences.

The authors also would like to thank ARC foundation which allowed Dr. SGARD to get a fellowship for a year of research during which he was able to carry out this study.

Funding information The authors state that this work has not received any funding.

Compliance with ethical standards

Guarantor The scientific guarantor of this publication is Aurélie Kas, MD, PhD, Department of Nuclear Medicine, Pitié-Salpêtrière C. Foix Hospital, APHP, Paris, France. Phone: 33 1 42 17 62 80. Fax: 33 1 42 17 62 92. Email: aurelie.kas@gmail.com

Conflict of interest The authors of this manuscript declare relationships with the following companies:

Maya Khalifé received a research grant from GE Healthcare.

Brice Fernandez and Gaspar Delso are GE Healthcare employees. Only non-GE employees had control of inclusion of data and information that might present a conflict of interest for authors who are employees of GE Healthcare. No other potential conflict of interest relevant to this article was reported.

Aurélie Kas received honoria for lectures from GE Healthcare and Piramal.

Marie-Odile Habert received honoraria for lectures from Lilly.

Statistics and biometry One of the authors has significant statistical expertise.

No complex statistical methods were necessary for this paper.

Informed consent Written informed consent was obtained from all subjects (patients) in this study.

Ethical approval Data of this study were extracted from the PET/MR examinations database of the Pitié-Salpêtrière Hospital, Paris, France, which was approved by the French authority for the protection of privacy and personal data in clinical research (CNIL, approval no. 2111722). All procedures performed in this study were in accordance with the ethical standards of the institutional research committee and with the 1964 Helsinki Declaration and its later amendments.

Methodology
- Retrospective
- Experimental
- Performed at one institution

References

1. Barthel H, Schroeter ML, Hoffmann K-T, Sabri O (2015) PET/MR in dementia and other neurodegenerative diseases. Semin Nucl Med 45:224–233. https://doi.org/10.1053/j.semnuclmed.2014.12.003

2. Ladefoged CN, Law I, Anazodo U et al (2017) A multi-centre evaluation of eleven clinically feasible brain PET/MRI attenuation correction techniques using a large cohort of patients. Neuroimage 147:346–359. https://doi.org/10.1016/j.neuroimage.2016.12.010
3. Sekine T, Buck A, Delso G et al (2015) Evaluation of atlas-based attenuation correction for integrated PET/MR in human brain – application of a head atlas and comparison to true CT-based attenuation correction. J Nucl Med 57:215–220. https://doi.org/10.2967/jnumed.115.159228
4. Burgos N, Cardoso MJ, Thielemans K et al (2014) Attenuation correction synthesis for hybrid PET-MR scanners: application to brain studies. IEEE Trans Med Imaging 33:2332–2341. https://doi.org/10.1109/TMI.2014.2340135
5. Sekine T, Burgos N, Warnock G et al (2016) Multi atlas-based attenuation correction for brain FDG-PET imaging using a TOF-PET/MR scanner– comparison with clinical single atlas- and CT-based attenuation correction. J Nucl Med 57:1258–1264. https://doi.org/10.2967/jnumed.115.169045
6. Khalifé M, Fernandez B, Jaubert O et al (2017) Subject-specific bone attenuation correction for brain PET/MR: can ZTE-MRI substitute CT scan accurately? Phys Med Biol 62:7814–7832. https://doi.org/10.1088/1361-6560/aa8851
7. Delso G, Kemp B, Kaushik S et al (2018) Improving PET/MR brain quantitation with template-enhanced ZTE. NeuroImage 181:403–413. https://doi.org/10.1016/j.neuroimage.2018.07.029
8. Delso G, Kemp B, Kaushik S, Wiesinger F, Sekine T (2015) Clinical evaluation of zero-echo-time MR imaging for the segmentation of the skull. J Nucl Med 56:417–422. https://doi.org/10.2967/jnumed.114.149997
9. Sekine T, Ter Voert EE, Warnock G et al (2016) Clinical evaluation of zero-echo-time attenuation correction for brain 18F-FDG PET/MRI: comparison with atlas attenuation correction. J Nucl Med 57:1927–1932. https://doi.org/10.2967/jnumed.116.175398
10. Wollenweber SD, Ambwani S, Delso G et al (2013) Evaluation of an atlas-based PET head attenuation correction using PET/CT amp; MR patient data. IEEE Trans Nucl Sci 60:3383–3390. https://doi.org/10.1109/TNS.2013.2273417
11. Wiesinger F, Sacolick LI, Menini A et al (2016) Zero TE MR bone imaging in the head. Magn Reson Med 75:107–114. https://doi.org/10.1002/mrm.25545
12. Delso G, Fernandez B, Wiesingern F, Jian Y, Bobb C, Jansen FP (2017) Repeatability of ZTE bone maps of the head. IEEE Transactions on Radiation and Plasma Medical Sciences pp 1-1
13. Yang J, Wiesinger F, Kaushik S et al (2017) Evaluation of sinus/edge-corrected zero-echo-time-based attenuation correction in brain PET/MRI. J Nucl Med 58:1873–1879. https://doi.org/10.2967/jnumed.116.188268
14. Tustison NJ, Avants BB, Cook PA et al (2010) N4ITK: improved N3 bias correction. IEEE Trans Med Imaging 29:1310–1320. https://doi.org/10.1109/TMI.2010.2046908
15. Wiesinger F, Bylund M, Yang J et al (2018) Zero TE-based pseudo-CT image conversion in the head and its application in PET/MR attenuation correction and MR-guided radiation therapy planning. Magn Reson Med. https://doi.org/10.1002/mrm.27134
16. Jenkinson M, Smith S (2001) A global optimisation method for robust affine registration of brain images. Med Image Anal 5:143–156
17. Burger C, Goerres G, Schoenes S, Buck A, Lonn AH, Von Schulthess GK (2002) PET attenuation coefficients from CT images: experimental evaluation of the transformation of CT into PET 511-keV attenuation coefficients. Eur J Nucl Med Mol Imaging 29:922–927. https://doi.org/10.1007/s00259-002-0796-3
18. Carney JPJ, Townsend DW, Rappoport V, Bendriem B (2006) Method for transforming CT images for attenuation correction in PET/CT imaging. Med Phys 33:976–983. https://doi.org/10.1118/1.2174132
19. Alessio AM, Kinahan PE, Cheng PM, Vesselle H, Karp J (2004) PET/CT scanner instrumentation, challenges, and solutions. Radiol Clin North Am 42:1017–1032, vii. https://doi.org/10.1016/j.rcl.2004.08.001
20. Zhang B, Pal D, Hu Z et al (2009) Attenuation correction for MR table and coils for a sequential PET/MR system. In: 2009 IEEE Nuclear Science Symposium Conference Record (NSS/MIC). pp 3303–3306
21. Eldib M, Bini J, Faul DD, Oesingmann N, Tsoumpas C, Fayad ZA (2016) Attenuation correction for MR coils in combined PET/MR imaging: a review. PET Clin 11:151–160. https://doi.org/10.1016/j.cpet.2015.10.004
22. Yakushev I, Landvogt C, Buchholz HG et al (2008) Choice of reference area in studies of Alzheimer's disease using positron emission tomography with fluorodeoxyglucose-F18. Psychiatry Res 164:143–153. https://doi.org/10.1016/j.pscychresns.2007.11.004
23. Tzourio-Mazoyer N, Landeau B, Papathanassiou D et al (2002) Automated anatomical labeling of activations in SPM using a macroscopic anatomical parcellation of the MNI MRI single-subject brain. NeuroImage 15:273–289. https://doi.org/10.1006/nimg.2001.0978
24. Sousa JM, Appel L, Engström M et al (2018) Evaluation of zero-echo-time attenuation correction for integrated PET/MR brain imaging-comparison to head atlas and 68Ge-transmission-based attenuation correction. EJNMMI Phys 5:20. https://doi.org/10.1186/s40658-018-0220-0
25. Rezaei A, Schramm G, Willekens SMA, Delso G, Van Laere K, Nuyts J (2019) A quantitative evaluation of joint activity and attenuation reconstruction in TOF-PET/MR brain imaging. J Nucl Med. https://doi.org/10.2967/jnumed.118.220871
26. Leynes AP, Yang J, Wiesinger F et al (2017) Direct PseudoCT generation for pelvis PET/MRI attenuation correction using deep convolutional neural networks with multi-parametric MRI: zero echo-time and Dixon deep pseudoCT (ZeDD-CT). J Nucl Med 57:jnumed.117.198051. https://doi.org/10.2967/jnumed.117.198051
27. Arabi H, Zeng G, Zheng G, Zaidi H (2019) Novel adversarial semantic structure deep learning for MRI-guided attenuation correction in brain PET/MRI. Eur J Nucl Med Mol Imaging. https://doi.org/10.1007/s00259-019-04380-x
28. Hwang D, Kim KY, Kang SK et al (2018) Improving the accuracy of simultaneously reconstructed activity and attenuation maps using deep learning. J Nucl Med 59:1624–1629. https://doi.org/10.2967/jnumed.117.202317
29. Ladefoged CN, Marner L, Hindsholm A, Law I, Højgaard L, Andersen FL (2019) Deep learning based attenuation correction of PET/MRI in pediatric brain tumor patients: evaluation in a clinical setting. Front Neurosci:12. https://doi.org/10.3389/fnins.2018.01005